Spring 2014

Structure and function of novel RTX-like proteins BAV1944 and BAV1945 in Bordetella avium

Nathaniel Tate Burkholder
James Madison University

Structure and function of novel RTX-like proteins BAV1944 and BAV1945 in *Bordetella avium*

A project presented to the faculty of the undergraduate College of Integrated Sciences and Engineering and College of Science and Mathematics

James Madison University

In partial fulfillment of the requirements for the degree of Bachelor of Science

Nathaniel Tate Burkholder

May 2014

Accepted by the faculty of the Department of Integrated Science and Technology and the Department of Biology, James Madison University, in partial fulfillment of the requirements for the Degree of Bachelor of Science. Presented at the ISAT Spring Symposium on April 11, 2014.

FACULTY COMMITTEE:

Project Advisor: Louise Temple, Ph.D.,
Professor, Integrated Science and Technology

Reader: Stephanie Stockwell, Ph.D.,
Assistant Professor, Integrated Science and Technology

Reader: Nathan Wright, Ph.D.,
Assistant Professor, Chemistry and Biochemistry

HONORS PROGRAM APPROVAL:

Barry Falk, Ph.D.,
Director, Honors Program

Table of Contents

List of Figures

Figures

Tables

Acknowledgements

My research has always been a collaborative effort, as even while I work alone I am using the tools and skills that I have obtained from the amazing faculty and students around me. I thank Dr. Temple for yanking me into this wonderful world of microorganisms six years ago and engaging me in following scientific pursuits that I hope will never end in my lifetime. I thank Dr. Stockwell for showing me the ropes of the lab and holding my hand whenever I had a million and one questions to ask. I thank Dr. Wright for showing me a new way of looking at biological molecules through physical means. I would also like to thank Dr. Raab, Dr. McKown, Dr. Scott, Dr. Miyamoto, and all the students who have worked with me in the lab over these last six years and helped provide me the means to accomplish anything I dared to try. Even the slightest contributions either intentionally or unintentionally have had significant effects on my development as a researcher. I would also like to thank the Department of Integrated Sciences and Technology for providing the facilities and support for conducting my research. I would like to thank my family as well for supporting my enrollment here at JMU and my summer research experiences every year, as these events have played vital roles in the completion of my thesis. Finally, I would like to acknowledge the vast amount of scientific knowledge passed down through literature that has served as the building blocks for my thesis work.

Abstract

Bordetella avium is a gram-negative bacterial pathogen that colonizes the upper trachea of turkeys and causes bordetellosis. Two large, novel proteins denoted as BAV1944 (447 kDa) and BAV1945 (650 kDa) are suspected to play a role in *B. avium* virulence. BAV1944 and BAV1945 appear to be secreted through an atypical SecA-dependent type I secretion system and have GD-rich nonapeptide repeats that are signature features of RTX proteins. BAV1945 also has a domain of unknown function that shares structural similarity to the self-processing cysteine protease domains in *Clostridium difficile* toxin B and the multifunctional autocatalytic repeat-in-toxin (MARTX) toxin in *Vibrio cholera*. We found that *bav1945* and the first gene of the type I secretion system, *bav1940*, are transcribed at 37°C, implicating their expression under normal host physiological temperatures. However, a derivative of 197N-2 lacking the *bav1944* and *bav1945* genes (Δ*bav1944-5*) exhibited wild-type levels of growth, serum resistance, tracheal binding affinity, and production of ciliary apoptosis. Our results may suggest that BAV1944 and BAV1945 act as supplementary toxins during infection as opposed to being primary virulence factors.

Introduction

Bordetella avium is a gram-negative pathogen that infects the upper respiratory tract of a wide range of wild and domesticated avian species (Skeeles, 1997). *B. avium* is an opportunistic pathogen in chickens, but domestic turkeys are the largest known reservoir for *B. avium* (Jackwood, 1995). Bordetellosis in turkeys is associated with sneezing and nasal discharge (Pitman, 1979). *B. avium* preferentially binds ciliated tracheal epithelial cells (Arp, 1984) similar to other *Bordetella* species (Rhea, 1915). Upon infection, *B. avium* reduces ciliary activity and induces apoptosis (Miyamoto, 2011). *B. avium* is of economic importance to the poultry industry as infection lowers the immune system increasing risk from secondary infection (Jackwood, 2003).

Infectious *Bordetella* cause similar disease in a variety of hosts, which allows well-characterized organisms like *B. pertussis* and *B. bronchiseptica* to be valuable for identifying potential virulence factors in *B. avium*. *B. pertussis* is the cause of whooping cough in humans and *B. bronchiseptica* is a major pathogen in mammals. *B. avium* is the furthest related member of the *Bordetella* genus based on DNA sequence homology (DeLey, 1986). *B. avium* is more phylogenetically similar to *B. bronchiseptica* indicated by the presence of more functional genes than *B. pertussis* (Sebaihia, 2006), which may help explain why *B. avium* and *B. bronchiseptica* have broader host ranges. *B. avium* lacks adhesins and toxins identified as virulence factors in *B. bronchiseptica* and *B. pertussis*, including the well-characterized pertussis toxin (Sebaihia, 2006). *B. avium* LPS and tracheal cytotoxin, which are common virulence factors in *Bordetella*, were not found to induce ciliary apoptosis (Miyamoto, 2011). Adenylate cyclase toxin (ACT) is another major virulence factor of *Bordetellae* (reviewed by Carbonetti, 2010), but only a truncated, nonfunctional form of ACT is produced by *B. avium* (Gentry-Weeks, 1988). *B. avium*

does produce hemagglutination factors that play a role in attachment (Temple, 2010), a tracheal cytotoxin similar to that in *B. pertussis*, and a lethal dermonecrotic toxin (Gentry-Weeks, 1988). Even though these pathogens cause similar symptoms, they utilize different virulence factors for infection.

Two novel genes, *bav1944* and *bav1945*, encode large proteins of unknown function. BAV1944 (4342 AA, 447 kDa) and BAV1945 (6460 AA, 650 kDa) share low amino acid homology to adhesins, hemolysins, and hemaglutinins found in other pathogenic bacteria. Virulence factors are often secreted proteins since they need to be exposed to the surface of the host cells. We believe that *bav1944* and *bav1945* are transcribed in an operon with the downstream genes *bav1940-3* (Fig. 1). The *bav1940-3* genes encode a putative type I secretion system (TISS), which has been predicted to be responsible for export of BAV1944 and BAV1945 (Sebaihia, 2006). Adem et. al have proposed a model for the assembly of this putative TISS (Fig. 2). Many well-known virulence factors like hemolysin A in *E. coli* are secreted by TISS's (Holland, 1990). We have predicted that BAV1944 and BAV1945 play some role in interacting with the host or environment either as surface associated or released factors.

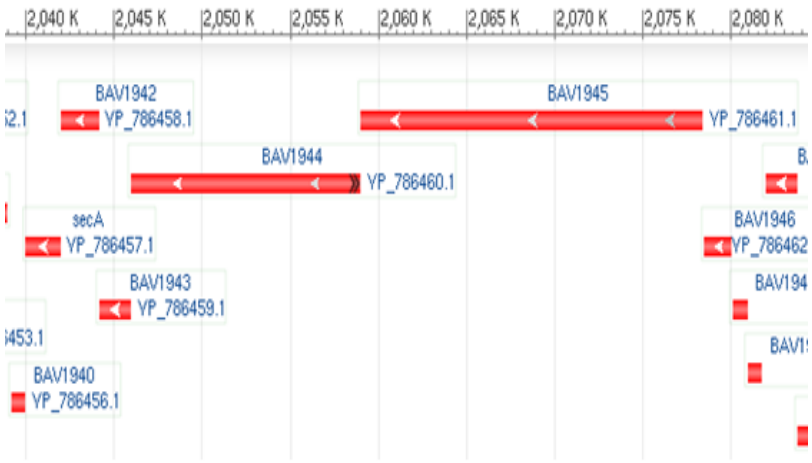

Figure 1. Large, secreted protein encoding regions *bav1944* and *bav1945* flanked by a type I secretion system (TISS) consisting of *bav1940*, *secA*, *bav1942*, and *bav1943*. These genes are transcribed on the Crick strand (reverse direction) and are predicted to be in an operon.

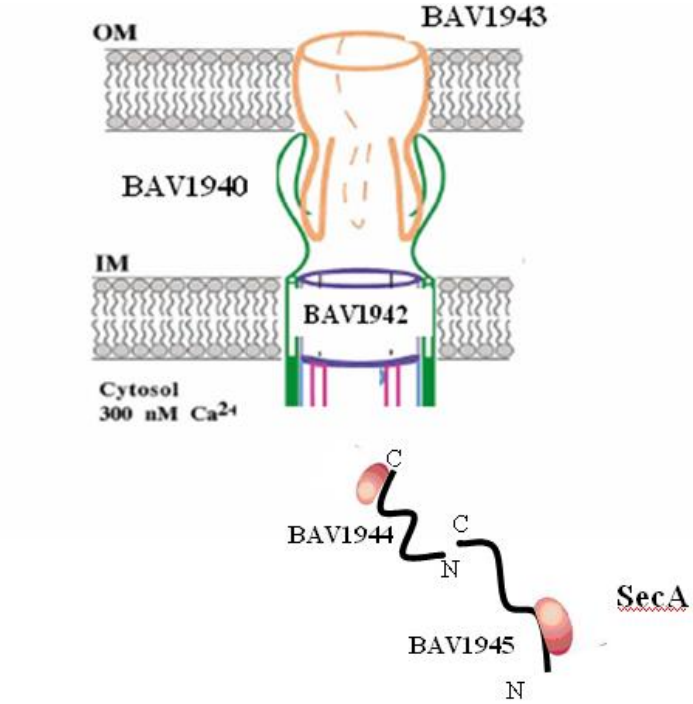

Figure 2. Diagram of putative TISS in *B. avium* believed to be involved in secretion of BAV1944 and BAV1945 (Adem, 2011).

To determine whether BAV1944 and BAV1945 play a role in *B. avium* pathogenesis, we investigated the expressional profile of *bav1945* and *bav1940* as well as determining the virulence profile of a *B. avium* mutant lacking *bav1944* and *bav1945* (Δ*bav1944-5*). Thermo regulation of virulence factor expression is a common tactic utilized by pathogens to balance energy consumption and infectivity. Results from previous microarray studies indicated that these *bav1944* and *bav1945* are expressed at 37°C, which is normal for host physiological temperatures. We confirmed these results using reverse transcription PCR (RT-PCR) with primers specific for *bav1945* and the first gene of the putative TISS, *bav1940*. We generated a Δ*bav1944-5* mutant through homologous recombination of a plasmid borne deletion construct onto the chromosome of *B. avium* 197N-2. We first examined the growth of Δ*bav1944-5* to see whether loss of these genes would be harmful to the cells or conferred a selective advantage in rich media. We then tested the serum resistance, tracheal attachment, and production of ciliary apoptosis of Δ*bav1944-5* to see if BAV1944 or BAV1945 were required for these virulence phenotypes.

Materials and Methods

Bacterial strains and culture conditions.

All bacterial strains and plasmids employed in this study are listed in Table 1. *E. coli* strains were grown in Luria-Bertani (LB) broth or agar (Difco) at 37°C. *B. avium* growth conditions were followed as previously described (Temple, 1998) in brain heart infusion (BHI), LB, or MacConkey media (Difco). Prior to turkey tracheal attachment assays, *B. avium* cells were grown on Bordet Gengou (BG) agar supplemented with 15% defibrinated sheep's blood. Antibiotics were included, when appropriate, at the following concentrations: ampicillin, 100 μg/ml; kanamycin, 30 μg/ml for *E. coli* and 150 μg/ml for *B. avium*; nalidixic acid, 30 μg/ml; streptomycin, 50 μg/ml.

DNA manipulations and genetic techniques

Primers synthesis and DNA sequencing were carried out at Elim Biopharmaceuticals (Hayward, CA). Primer sequences can be found in Table 2. Plasmid DNA was isolated using either the QIAprep spin miniprep kit (Qiagen, Valencia, CA) or Zyppy plasmid miniprep kit (Zymo Research, Irvine, CA). Restriction endonucleases were purchased from New England BioLabs (Ipswich, MA). Gel purification of DNA fragments was performed using the QIAquick gel extraction kit (Qiagen). Ligation reactions were performed using T4 DNA Ligase (NEB). PCRs were performed using Advantage GC cDNA Polymerase (Clontech, Mountain View, CA) and approximately 1nM of each primer. Chromosomal preparations of *B. avium* wild-type and mutant strains were made using Quick g-DNA Miniprep kits (Zymo). PCR products were resolved by agarose electrophoresis and gel purified. *E. coli* strains DH5α, Top10 (NEB), MC4100λPir, and T7 Express *lysY* (NEB) listed in Table 1 were treated with $CaCl_2$ and used as

recipients in transformation experiments. All methods were performed according to the manufacturer's instructions.

Nucleic acid electrophoresis

Nucleic acids were separated on agarose gels (1% agarose, 1x tris acetate/EDTA, 0.4 μg/ml ethidium bromide) using gel electrophoresis. 1 kb DNA Ladder (NEB) was prepared (1 μg/μl stock, 20 mM NaCl, 1x loading dye, diH_2O) and run alongside samples. Gels were run at approximately 100V for 30 min, and visualized under UV light. Desired bands for cloning purposes were cut out and purified based on standardized protocols (Qiagen/Zymoclean).

RNA Extraction from *B. avium* cultures.

Cultures of *B. avium* were grown at 37°C shaking up to mid-log phase (OD600 = 0.4-0.6) and 50mL of each was harvested through centrifugation. Pellets were either used for RNA extraction or stored immediately at -70°C. RNA was extracted from pellets with TRIzol (Invitrogen) and the RNA Extraction kit (Zymo) using a modified protocol as follows: Pellets were resuspended in 300μL of TRIzol, mixed, and centrifuged in a table-top centrifuge at max speed for 1 min. After the supernatant was moved to a Zymo Spin-Away column the remaining protocol was followed according to the manufacturer's instructions, including an optional on-column DNase procedure. Approximately 1μg of RNA was run on 1.2% agarose gels to ensure quality. Total RNA samples were checked for DNA contamination using approximately 500ng in a PCR using RT-PCR primers from Table 2. Reactions were run with one cycle of 95°C for 5 min, 30 cycles of 95°C for 30 sec, 58°C for 30 sec, 72°C for 1 min, and one cycle of 72°C for 5 min. RNA was extracted from cultures grown at 25°C or with 20 mM $MgSO_4$, but RT-PCR was not followed as DNA could not be removed under these conditions.

RT-PCR of *bav1945* and *bav1940*.

Complementary DNA (cDNA) of *bav1945* and *bav1940* were synthesized using purified total RNA and the following protocol: 1µL of RNA (~500 ng), 1µL of reverse primer, 1µL of 10mM dNTP mix, and 7µL of DEPC treated water were mixed and incubated at 65°C for 5 min. The samples were then placed on ice while 1µL of Superscript III Reverse Transcriptase (Invitrogen), 1µL of RNase OUT (Invitrogen), 2µL of 10x RT buffer, 4µL of 25mM $MgCl_2$, and 2µL of 0.1M DTT were added to each. The samples were incubated at 50°C for 1h followed by 85°C for 5 min to terminate the RT reaction. Approximately 2µg of cDNA was used in PCR reactions for both *bav1945* and *bav1940* using the same protocol as above. Determination of a quantitative critical point was not pursued due to contaminating bands for both products.

Deletion mutation construction.

B. avium 197N genomic DNA was used as a template for amplification of the upstream and downstream regions of the *bav1940-43* and *bav1944-45* loci using primers listed in Table 2. Reactions were run with one cycle of 95°C for 5 min, 30 cycles of 95°C for 30 sec, 55°C for 30 sec, 72°C for 1-2 min (for 1kb or 2kb products respectively), and one cycle of 72°C for 5 min. The respective amplified fragments were fused together through SOE-PCR and ligated into pCR2.1. The ligation mixtures were transformed into $CaCl_2$ competent DH5α cells via heat shock and selected on ampicillin and 5-bromo-4-chloro-3-indolyl-β-D-galactopyranoside (0.5µg/ml). Successful insertion of the desired constructs was confirmed by restriction digest using *Eco*RI and sequencing. The Δ*1940-43* and Δ*1944-45* constructs were cut out with *Eco*RI and ligated into similarly cut pKAS46. The ligation mixtures were transformed into electrically

competent MC4100λPir cells via electroporation and selected on kanamycin. Successful insertion of the desired regions was confirmed by restriction digest.

Allelic Replacement.

Suicide vector pKAS46 (Δ*bav1944-45)* was transferred to *B. avium* through tri-parental mating. A 197N-2 derivative with a plasmid carrying $MgSO_4$ inducible recombination genes *recE* and *recT* was used as the recipient. *B. avium* and *E. coli* strains carrying the recombinant plasmid and conjugation plasmid pRK2013 were mixed in 10:1:1 ratios respectively. Suspensions were puddled onto 1x PBS plates with 20mM $MgSO_4$ for 12h and swabbed onto antibiotic selective media. Merodiploid strains were identified through kanamycin resistance (Kan^{150}) and streptomycin sensitivity (Str^{50}). Streptomycin sensitivity of exconjugants was determined through spotting serial dilutions of culture grown in appropriate antibiotics (Nal^{30} for 197N-2 and $Nal^{30}Kan^{150}$ for exconjugants). Exconjugants were selected for by loss of kanamycin resistance and recovery of streptomycin resistance after passaging in the absence of antibiotics. A mutant *B. avium* strain deficient in the *bav1944-45* locus was identified through PCR using primers for internal region of the Δ*1944-45* construct. A new primer set for detecting the Δ*1944-45* construct was devised due to nonspecific binding in PCR with *B. avium* genomic DNA. PCR with primers for *bav1945* were used to further confirm loss of this locus. *B. avium* 197N-2 and Δ*bav1944-5* cultures were grown at 37°C shaking with $Nal^{30}Str^{50}$ for all experiments.

Growth curve.

Overnight starter cultures of 197N-2 and Δ*bav1944-5* were used to inoculate 25mL of fresh LB at 1:50 dilutions. Cultures were monitored hourly for OD_{600} readings. Each strain was tested in triplicate.

Serum resistance assay.

Cultures of 197N-2, Δ*bav1944-5*, and Δ*wlb* were grown up to OD_{600} = 0.5 (~10^9 cfu/mL), harvested by centrifugation, and washed twice with PBS. Cell suspensions were diluted to approximately 10^7 cfu/mL. Serum reactions were made by mixing 16µL of diluted cells, 64µL of PBS, and 80µL of naïve turkey poult serum (Cocalico). Heat inactivated serum (incubated at 56°C for 30 min) was added to another set of reactions and run in parallel. A 10µL aliquot of each reaction was removed immediately to determine the initial viable bacterial cell count from colony forming unit (cfu) counts. The mixture was then incubated at 37°C for 1h. Bacterial cell counts were determined through serial dilutions and plating onto MacConkey agar. The degree of serum resistance was quantified by determining the percent of the initial population that survived the serum treatment. Trials were run in duplicate (except for a mutant known to be deficient in serum resistance, which was added for the second trial to test serum quality).

Hemagglutination assay.

Hemagglutination assays were run as a preliminary test for tracheal attachment ability due to the correlation of these two phenotypes in *B. avium* strains and the ease of this type of assay. Cultures of 197N-2, Δ*bav1944-5*, and Δ*hagB* were struck out on Nal^{30} MacConkey agar plates for confluent overnight growth. Cells were resuspended in 1% NaCl up to OD_{600}=1 (~10^9 cfu/mL). Cell suspensions were concentrated 10^{11} cfu/mL through centrifugation, removal of the supernatant, and resuspension in an appropriate volume of 1% NaCl. Serial dilutions of 1:1 bacterial solution and 1% NaCl were made in rows of 12 wells in 96-well pointed bottom plates. Settled 1% guinea pig erythrocyte solution (Cocalico) was added in 1:1 ratios with bacterial

dilutions (100µL final volume) and mixed gently. Plates were covered in parafilm to reduce evaporation and stored at 4°C overnight before observation. Each strain was tested in duplicate.

Tracheal attachment assay.

Cultures of 197N-2, Δ*bav1944-5*, and Δ*hagB* were struck out on BG-blood plates for confluent overnight growth. Cells were suspended in 1x EBSS up to OD_{600}=0.5 and diluted to 10^7 cfu/mL for tracheal ring inoculations. Cell suspensions were further diluted in PBS/1% Triton X-100 and plated onto MacConkey agar to determine initial bacterial concentrations. Turkey poults incubated for ~26 days were euthanized and dissected. Tracheal rings of approximately 2mm were excised and washed in EBSS three times. In 6-well microtitre plates, 5-6 tracheal rings were mixed with 0.5 mL of 10^7 cfu/mL bacterial suspensions. The plates were rocked in a 42°C hybridization oven for 1h. After incubation, the supernatant from each well was removed and replaced with 0.5 mL of fresh EBSS to wash the rings. This wash step was repeated 3 times with a 2 min incubation period at 42°C between each. Individual rings were placed in tubes containing 1mL of PBS/1% Triton X-100 for overnight storage at 4°C. The tubes were then vortexed for 5 min to remove any remaining attached bacteria from the tracheal rings. The bacterial solutions were serial diluted and plated onto MacConkey agar to quantify the percent of cells that attached. Each strain was tested in triplicate (3 sets of 5-6 rings).

Collagen coated coverslips.

Collagen coated coverslips were prepared for setting tracheal rings. The coverslips were first washed in 70% EtOH with 1mM HCl and blot dried. The coverslips were then washed in a 0.01% poly-lysine solution, blot dried, and autoclaved. A collagen gel solution (pH 7.4) was prepared with 2 mL of Nutragen collagen solution (Advanced BioMatrix, San Diego, California),

0.5mL of 10x EBSS, 150µL of 7.5% $NaHCO_3$, and 0.5mL of 1M NaOH. The coverslips were coated with 200µL of collagen gel solution spread evenly over the surface in 6-well culture plates. The collagen coverslips were incubated at 37°C for 1-3h and then covered with 2-3mL of EBSS. Plates were stored at 37°C with 5% CO_2 within 24h of use.

Tracheal ring explant cultures.

Tracheal rings from 26-day old embryonated turkey eggs were extracted and prepared as before. Five tracheal rings were transferred to each collagen coated coverslip. The plates were incubated at 37°C with 5% CO_2 for 1h. M199 media supplemented with 5% fetal bovine serum and 1% antibiotics/antimycotics was used to cover the tracheal rings and provide nutrients for newly growing ciliated cells. The plates were incubated at 37°C with 5% CO_2 over the course of a week while changing the out the media every 2 days. When changing the media, cellular debris was removed through aspiration.

Bacterial inoculation and annexin staining.

Cultures of 197N-2 and Δ*bav1944-5* were struck out on Bordet-Gengou-blood plates for confluent overnight growth. Dense cell suspensions were made in EBSS, vortexed for 5 min, and centrifuged to separate whole cell and extracellular fractions. The supernatants were filter sterilized to remove any remaining cells, and 20mM $CaCl_2$/20mM $MgSO_4$ was added to potentially enhance BAV1944/1945 activity. The pellets were resuspended in EBSS and normalized to OD_{600} = 0.5. EBSS, 10^8 of whole cell resuspension, or filtered supernatant was added to each well. The covered collagen coated coverslips (dang that is a lot of C's!) were incubated at 37°C with 5% CO_2 for 6h. After incubation, the treatment was removed and the rings were rinsed three times with PBS. The rings were then rinsed once with pre-warmed

(~37°C) annexin binding buffer. A staining solution containing 2% Annexin-V-FLUOS conjugate and 1% Propidium Iodide (Roche, Madison, Wisconsin) was added directly to the tracheal rings. The plates were incubated at 37°C shaking for 20 min. The rings were then rinsed with binding buffer, and the plates were covered to reduce light exposure. Annexin and PI staining were imaged under widefield fluorescence using a TE2000 Nikon microscope. Filter blocks with excitation = 450-490 nm/emission = 500-550 nm (green) and excitation = 534-546 nm/emission = 570-640 nm (red) were used. Fluorescence from wild-type *B. avium* exposure (197N-2) was used as a reference.

Statistical Analysis

The growth kinetics and phenotypic outputs of the 197N-2 and Δ*bav1944-5* strains were compared using independent student t-tests with a significance value of 0.05. Averages and standard deviations were determined using Microsoft Excel functions. The t-statistics were determined by subtracting the average values and dividing by the square root of the sum of variances over the degrees of freedom. The average absorbance of *B. avium* cultures at each time point was compared during growth trials. The average percent survival was analyzed for the serum resistance assays. Differences in hemagglutination were observed by eye, while percentages of attachment were compared in tracheal binding trials. The percentage of apoptotic ciliated cells in treated versus non-treated samples was not determined.

Results

Expression of *bav1945* and *bav1940*.

B. avium cultures were grown at 37°C to upregulate virulence factor expression. RNA was successfully isolated from *B. avium* cultures grown at 37°C as indicated by bands corresponding to the 18S (1kb) and 28S (2kb) ribosomal RNA subunits (Fig. S1). Complementary DNA of *bav1945* and *bav1940* transcripts was made using reverse transcriptase and primers for these loci. PCR reactions of the *bav1945* and *bav1940* cDNA samples resulted in the desired products 0.6 kb and 0.8 kb respectively (Fig. 3). However, the larger band of about 1.2 kb in the *bav1945* lane and the smaller band of about 0.4 kb in the *bav1940* lane appear to represent random amplification products (Fig. 3). These bands are not made when these primers are used on *B. avium* genomic DNA (data not shown), but only when used on cDNA. The *bav1945* locus appears to be expressed more than the *bav1940* locus due to more intense bands (Fig. 3). Therefore, there seems to be greater expression of the large secreted proteins compared to their TISS.

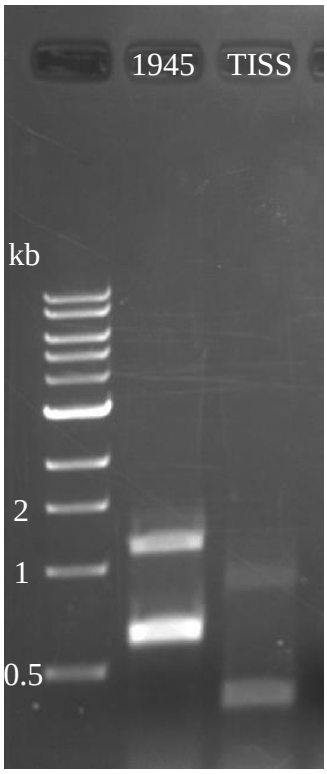

Figure 3. RT-PCR of cDNA made from *B. avium* grown at 37°C using primers for *bav1945* (lane 2) and *bav1940* (lane 3). A molecular weight standard was run in lane 1 with labelled bands at 0.5, 1, and 2 kb.

Construction of the Δ*bav1944-5* mutant.

The upstream and downstream coding elements of the *bav1944-5* locus were amplified as two bands of approximately 1.2 and 0.8 kb were resolved on agarose gels (Fig. S3.) These fragments were spliced together using PCR as shown by the resolved 2 kb fragment (Fig. S4). Cloning of the Δ*bav1944-5* fragment in pCR2.1was confirmed by restriction digest (Fig. S5) and sequencing. Digested Δ*bav1944-5* insert was purified, ligated to similarly cut pKAS46, and transformed into MC4100λ cells. Insertion into the vector was confirmed through release of the Δ*bav1944-5* fragment from purified plasmids (Fig. S6).The pKAS46 vector is not replicable in *B. avium* and encodes a kanamycin resistance gene for selection, which makes it a suitable shuttle vector for recombination in *B. avium*. Conjugational transfer of the pKAS46 (Δ*bav1944-*

5) construct into *B. avium* 197N-2 was initially selected for with high concentrations of kanamycin. However, colonies isolated on selective media were often found to not contain the insert sequence when tested with PCR (data not shown). The use of pKAS46, which encodes a functional ribosomal fragment that confers moderate streptomycin sensitivity, allowed for two forms of selection in streptomycin resistant 197N-2. A kanamycin resistant potential single-crossover was shown to have a 3-fold difference in streptomycin resistance compared to 197N-2 (Fig. 4). After passaging in the absence of antibiotics, a mutant containing the Δ*bav1944-5* sequence recombined in place of the *bav1944-5* locus was identified through genomic DNA PCR (Fig. 5).

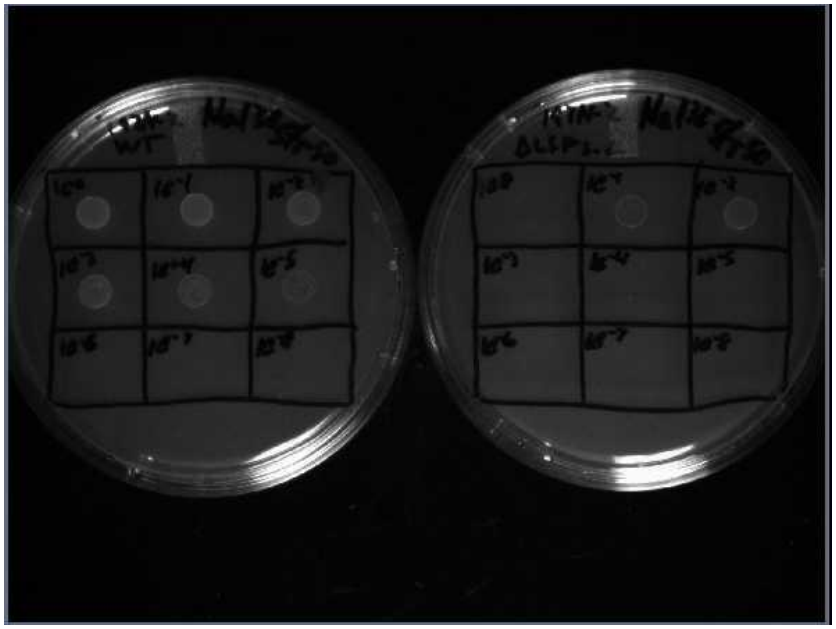

Figure 4. Streptomycin sensitivity assays of 197N-2 (left) and 197N-2/pKAS46 (Δ*bav1944-5*) single crossover mutant (right). Serial dilutions of overnight cultures were spotted onto plates containing streptomycin to show sensitivity conferred by pKAS46.

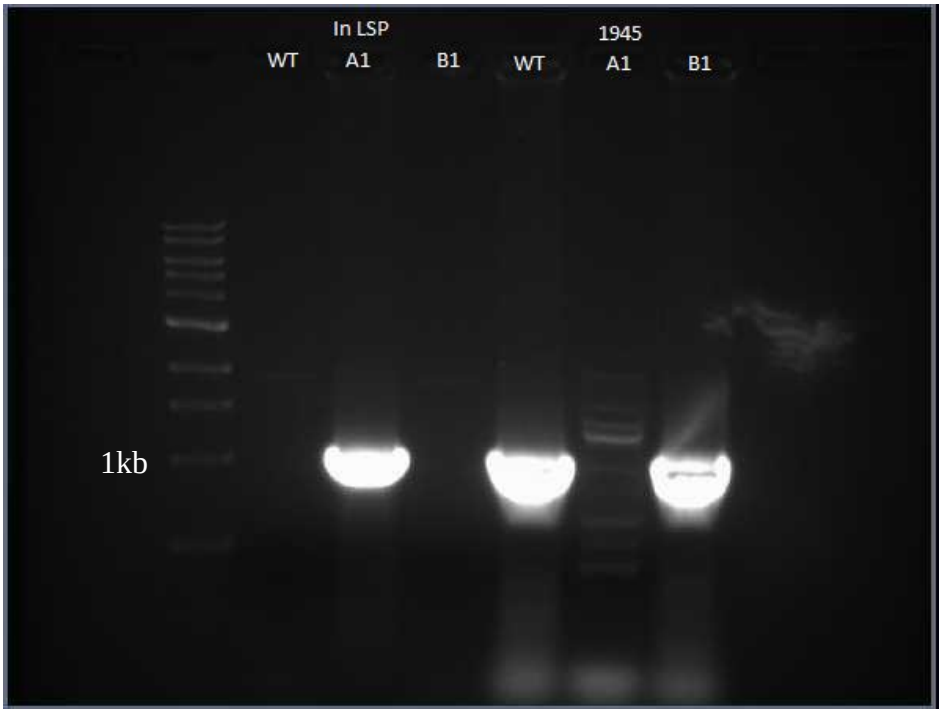

Figure 5. PCR confirmation of Δ*bav1944-5* construction. Extracted genomic DNA from 197N-2 (lanes 2 and 5) and potential Δ*bav1944-5* strains A1 (lanes 3 and 6) /B1 (lanes 4 and 7) was amplified with either In *bav1944-5* or *bav1945* primers. Genomic DNA from isolate A1 produced a band when amplified with the Δ*bav1944-5* primers instead of primers for the wild-type *bav1945* allele, indicating allelic replacement. A molecular weight standard was run in lane 1 with the band at 1 kb labelled.

Phenotypic assessment of Δ*bav1944-5* mutant.

There was no observable growth deficiency of the Δ*bav1944-5* mutant, which would have indicated that these genes were essential. In fact, Δ*bav1944-5* cultures were slightly more turbid at early log-phase (0.2-0.5 OD_{600}) compared to the *B. avium* 197N-2 strain even if not significantly different (Fig. 6). There was no significant defect in serum resistance of Δ*bav1944-5* compared to197N-2 (Fig. 7). We included *B. avium* Δ*wlb* as a control for ensuring serum activity as the survivability of this mutant is severely inhibited due to a lack of LPS. The Δ*bav1944-5* mutant exhibited wild-type levels of hemagglutination (Fig. 8) and tracheal

attachment (Fig. 9). These results agree with each other as hemagglutination and tracheal attachment are often attributed to the same virulence factors in *B. avium*. There was no observable difference in the amount of annexin staining between ciliated cultures treated with either Δ*bav1944-5* or 197N-2 (Fig. 10). Therefore, *bav1944-5* produced wild-type levels of ciliary apoptosis.

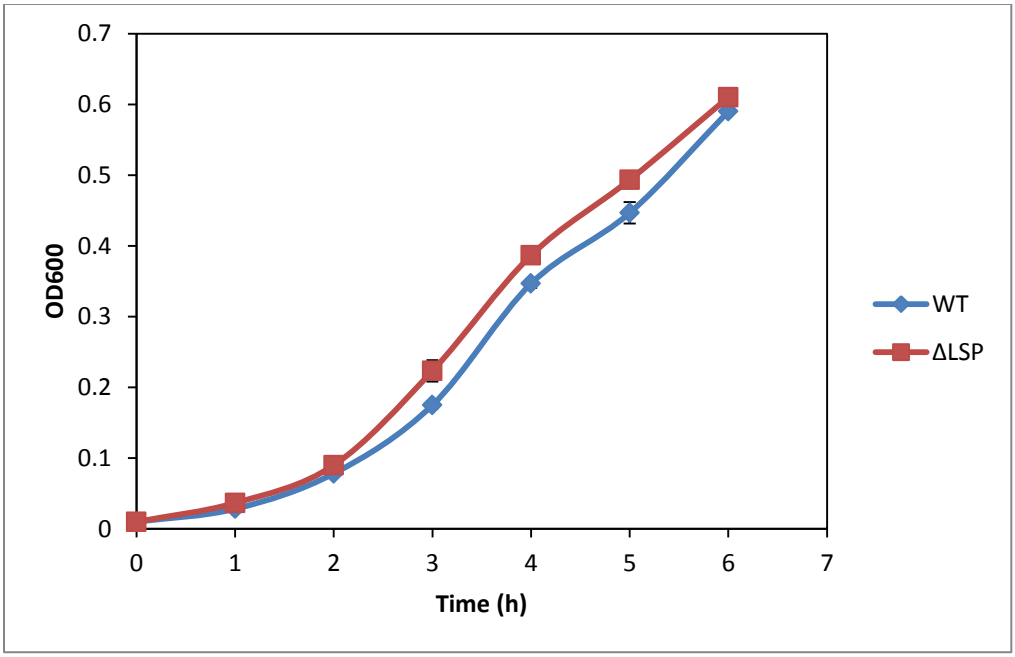

Figure 6. Growth curves of 197N-2 (WT) and Δ*bav1944-5* (ΔLSP). Three side-by-side flasks of media were inoculated with 1:50 overnight starter cultures. The average optical density at each time point was compared using a student's t-test. There was no significant deviation in optical density at any point during the time course (p=0.05).

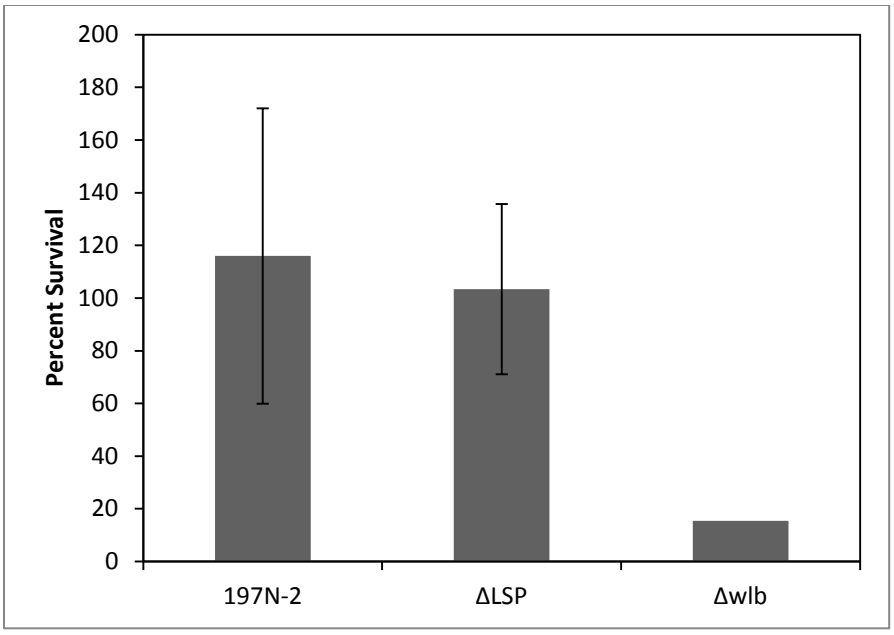

Figure 7. Serum resistance assays of 197N-2, Δ*bav1944-5* (ΔLSP), and Δ*wlb*. Percent survival was determined as the number of cells in pretreated samples minus the number of cells in post treated samples divided by the number of cells in heat inactivated samples. Each assay was conducted twice except for the Δ*wlb* mutant, which was used only in the second trial as a quality control (serum sensitive). There was no significant difference in the average percent survival between the 197N-2 and Δ*bav1944-5* strains using a student's t-test (p=0.05).

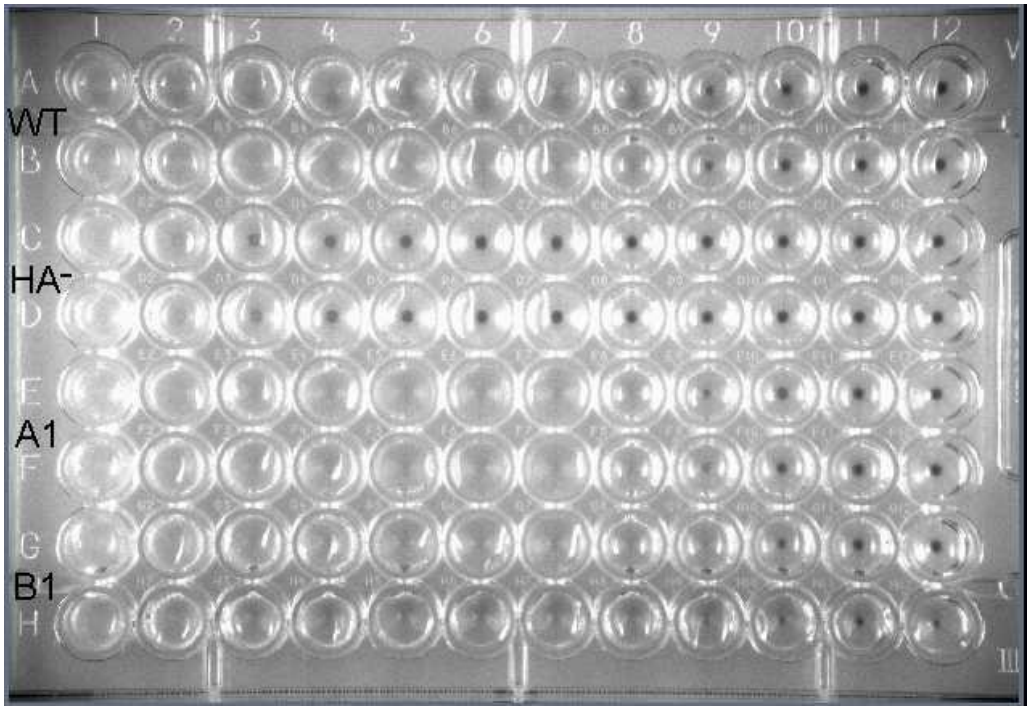

Figure 8. Hemagglutination assays of 197N-2 (WT), Δ*hagB* (HA-), Δ*bav1944-5* (A1), and a false positive mutant (B1). Each strain was tested in duplicate as pairs of lanes represent one treatment (e.g. 197N-2 was added to lanes A and B). Ten-fold serial dilutions from approximately 10^{11} cfu/mL culture resuspensions were added to wells with the same volume of erythrocyte solution. Serial dilutions were added from left to right (e.g. column 1 contains $5x10^{10}$ cfu/mL while column 2 contains $5x10^{9}$ cfu/mL). Formation of dense dots represents pelleting of red blood cells, while diffuse solutions represent hemagglutination. The Δ*hagB* strain served as a positive control for loss of hemagglutination due to increased red blood cell pelleting at higher bacterial cell concentrations (lanes C and D). Both 197N-2 and Δ*bav1944-5* cause hemagglutination when up to 100 cfu/mL are added to the erythrocyte solutions (lanes A, B, E, and F).

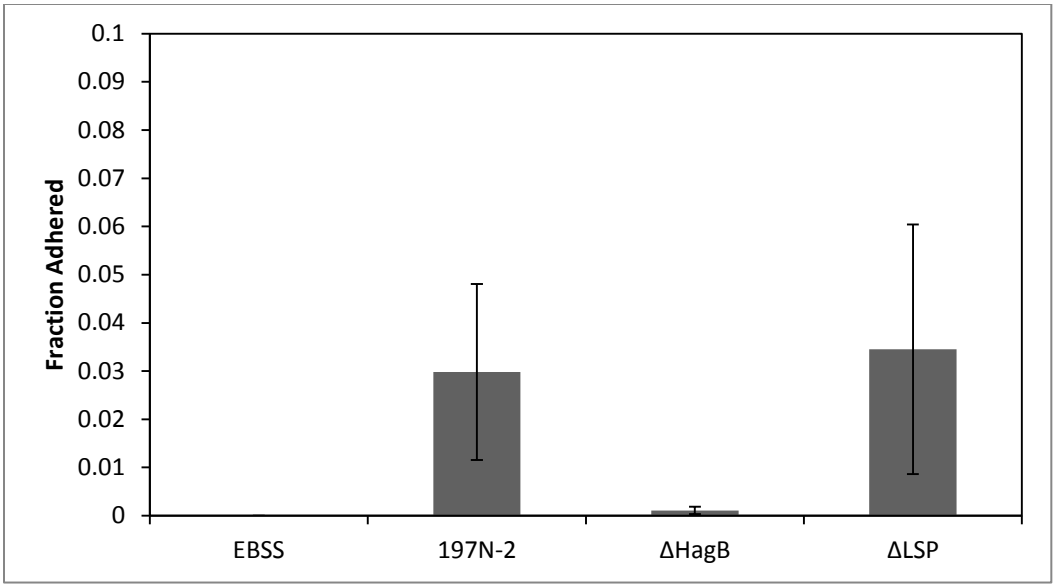

Figure 9. Tracheal attachment assays of 197N-2 (WT), Δ*hagB* (ΔHagB), and Δ*bav1944-5* (ΔLSP). The fraction of cells that adhered was determined as the number of cells collected post treatment divided by the number of cells used to inoculate tracheal rings. The Δ*hagB* strain served as a positive control for loss of attachment. Each condition was tested in triplicate (5-6 rings per trial). There was no significant difference in the average fraction of bound 197N-2 and Δ*bav1944-5* strains using a student's t-test (p=0.05).

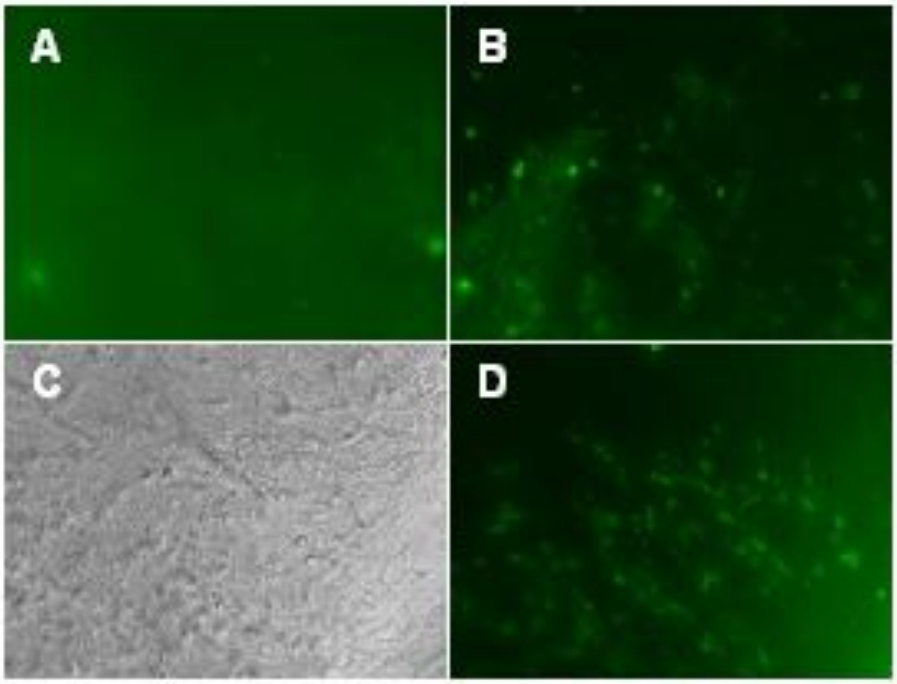

Figure 10. Representative DIC and fluorescent imaging of ciliated tracheal cells exposed to EBSS, whole cell 197N-2, or whole cell Δ*bav1944-5*. Tufts of cilia were observed under 20X DIC for activity and analyzed under green fluorescent light to detect annexin staining. Regions of concentrated fluorescence was indicative of apoptosis (see B and D), which were then compared with locations of live ciliary tufts (observed under DIC through real time). The sample conditions shown were of **A.** EBSS negative control **B.** 197N-2 wild type **C.** Δ*1944-5* DIC and **D.** Δ*1944-5*.

Discussion

The role of the large, secreted proteins BAV1944 and BAV1945 continues to be one of the most interesting questions in the field of *B. avium* pathogenesis. We believe that the putative operon consisting of *bav1940-5* is expressed during infection as it appears to be transcribed under normal lab conditions. Previous microarray results had indicated that these genes were upregulated under non-virulence conditions through growth modulation with $MgSO_4$ or at 25°C. However, we could not compare the transcription levels of the modulated cultures due to genomic DNA contamination of extracted RNA. We predict that the putative *bav1940-5* operon is upregulated during the early stages of pathogenesis. The complicating bands made during RT-PCR of *bav1945* and *bav1940* could represent processed RNA transcripts, which may implicate some form of transcriptional control of these genes during the later stages of pathogenesis. We initially tested the functionality of the BAV1944 and BAV1945 proteins through conducting various phenotypic analyses with the Δ*bav1944-5* mutant. Neither of these proteins are necessary for *B. avium* viability as Δ*bav1944-5* grew at wild-type levels. We did not find Δ*bav1944-5* to be deficient in serum resistance, tracheal attachment, and production of ciliary apoptosis, which are known attributes of virulent *B. avium*. These results could suggest that BAV1944 and BAV1945 serve as secondary virulence factors that promote pathogenesis.

BAV1945 and BAV1944 when combined by their amino acid sequences share significant homology with the very large, putative repeat-in-toxin (RTX) toxins found in *Achromobacter pichaudii* and *A. xylosoxidans*. RTX toxins display a wide variety of structural features and functions, but are typically found to be secreted by TISSs and have glycine/aspartate rich nonapeptide repeats (reviewed by Linhartova, 2010). The large *Clostridium difficile* toxins A and B (TcdA/B), *Vibrio cholerae* multifunctional autoprocessing RTX toxin ($MARTX_{VC}$), and

adenylate cyclase toxin (ACT) in *B. pertussis* may serve as models for describing BAV1944 and BAV1945. These large RTX toxins primarily facilitate host immune evasion through the disruption of actin organization in phagocytes (Kuehne, 2010; Fullner, 2000; Kamanova, 2008). The TcdB and $MARTX_{VC}$ also have an N-terminal cysteine protease domain, which shares structural homology to a domain of unknown function in BAV1945. We developed a working model for the potential activity of BAV1944 and BAV1945 within the context of these large RTX toxins.

We have predicted that BAV1944 and BAV1945 are secreted by a TISS encoded by the *bav1940-3* locus. RTX TISSs recognize approximately 60 residues on the C-terminal end of their respective toxins (Gentschev, 1990). The inner membrane component BAV1942 may be responsible for recognizing a sequence on either BAV1944 or BAV1945. BAV1940 shares homology to HlyD in *E. coli*, implicating its role as the transmembrane segment of the TISS. Adem et al. predicted that *bav1943* encoded the outer membrane component of this TISS (2011), but a more likely candidate is the upstream BAV1946 TolC-like protein. The TolC required for $MARTX_{VC}$ secretion is also encoded outside of the TISS locus (Fullner, 1999). Since BAV1943 shares similarity to signal transduction proteins, it may instead play a role in regulation of secretion system assembly and function.

The most unusual factor in the BAV1944 and BAV1945 TISS is the SecA encoded by *bav1941*. This factor likely acts as the ATP-hydrolyzing motor protein in this system since BAV1942 does not contain an ATP binding motif (Adem, 2011). Sec proteins are key components of TISSs that typically facilitate intermediate translocation into the periplasm as opposed to a single-step translocation observed in TISSs (Tseng, 2009). It is not uncommon to see atypical secretion systems associated with RTX-like proteins. The TISS utilized by *Vibrio* sp.

to export MARTX toxins encodes two ABC transporters that form a heterodimer as opposed to the traditional TISS ABC transporter homodimers (Boardman, 2004). However, there is no SecB-like factor encoded near the *bav1940-5* locus, which could facilitate trafficking through the secretion system (Weiss, 1988). Due to their large size, BAV1944 and BAV1945 may require a more controlled mode of secretion through an unknown mechanism. We do believe that BAV1944 and BAV1945 are secreted by an atypical TISS either through a single-step or intermediate translocation event.

Obtaining evidence of BAV1944 and BAV1945 protein expression and secretion would require some way of detecting the proteins directly. Purification by size or charge (approximate pI of 5.0) would seem feasible, but running these proteins on even a low percentage SDS-PAGE gel (4%) would be difficult due to their large size. Polyclonal antibodies were made against a predicted antigenic C-terminal peptide sequence from BAV1944. These antibodies were used in dot blots with fractionated *B. avium* protein samples, but the antibodies detected proteins only in the cytoplasm and membrane rather than in the secreted fraction (Adem, 2011). When we repeated these experiments we also cross-reactivity of the antibodies with pre-immune serum. If the observed data is valid, then the epitope is being expressed and remaining cell-associated or being cleaved off before secretion. It is also possible that there is not enough of BAV1944 or BAV1945 being secreted to detect on a blot due to secretion regulation or some unknown factor. Another promising avenue of detecting these proteins would be to use mass spectrometry to identify peaks corresponding to these large proteins in fractionated *B. avium* samples.

Large pore forming RTX toxins have signature GD-rich nonapeptide repeats in their C-termini (Ladant, 1999). These regions form β-rolls that bind calcium upon RTX toxin secretion (Baumann, 1993). Calcium binding in the host extracellular space induces proper folding, which

is thought to be necessary for targeting host membranes (Rose, 1995). For instance, the C-terminal domain in the ACT of *B. pertussis* is required for membrane binding and forming pores in host erythrocyte membranes (Gray, 1999). We found two repeats with the core RTX nonapeptide residues G-G-X-G-X-D in BAV1945 and six concentrated in the C-terminus of BAV1944 using Protein Pattern Search (Gene Infinity). We also found a more extensive GD-rich region of repetitive residues in the C-terminus of BAV1944 using RADAR (Fig. 11). HlyD in *E. coli* has been shown to be necessary for proper folding of HlyA by coupling calcium binding upon secretion (Pimenta, 2005). BAV1940 may then provide both a periplasmic channel for secretion and facilitate calcium binding by the C-terminal GD-rich region of BAV1944. Since it would appear that BAV1944 has a greater capacity to undergo calcium induced folding than BAV1945, BAV1944 may be responsible for directing BAV1945 to host membranes. BAV1944 could even form pores in the host membrane and allow BAV1945 to be transported into the host's cytosol.

Figure 11. BAV1944 C-terminal repetitive region identified by RADAR.

The ligands and mechanisms for host membrane binding of RTX toxins are still unclear. It has been suggested that large pore forming RTX toxins target glycosylated surface proteins commonly found on a wide range of cell types (Morova, 2008). However, pore forming toxins

like staphylococcoal alpha-hemolysin can target membranes devoid of embedded proteins (Song, 1996). Post-translational acylation prior to secretion has been implicated in productive binding of RTX toxins to their respective receptors (Linhartova, 2010). BAV1939 is a CaiB-like acyl-CoA transferase, which could catalyze acylation of BAV1944. The role of acylation in RTX toxin-receptor binding is currently under investigation in various labs.

BAV1945 has an N-terminal domain of unknown function that structurally resembles the C60 family of cysteine protease domains (Fig. 12). The cysteine protease domains (CPDs) in *C. difficile* TcdB and $MARTX_{VC}$ undergo self-cleavage to release cytotoxic glucosyltransferase domains into the host cytosol (Reineke, 2007 and Sheahan, 2007). Cysteine protease activity requires binding of inositol hexakiphosphate (IP6) for TcdB (Reineke, 2007) and $MARTX_{VC}$ (Prochazkova, 2008 and Lupardus, 2008). IP6 was not identified as a potential binding partner of the BAV1945 putative CPD when generating a model using Phyre^2, possibly suggesting that another host molecule is necessary for CPD induction. Both CPDs recognize N-terminal sequences consisting of LXXL|XXXX for $MARTX_{VC}$ (Shen, 2009) or XXL|GXX for TcdB (Rupnik, 2005). There are two potential cleavage sites on the N-terminus side of the BAV1945 CPD which consist of the residues LYSL|LSGK and LGGL|ATPT. The actual cleavage site could be determined using mass spectrometry or N-terminal sequencing of BAV1945 CPD cleavage products. We designed an expression construct carrying the *bav1945* nucleotides from 402-996 (594 bp) for isolating the BAV1945 CPD (229 AA, pI=5.05, 24.1 kDa). This purified cysteine protease could be used to examine the dynamics of BAV1945 self-processing. Antibodies could also be made for the BAV1945 CPD, which would be useful in tracking BAV1945 over the course of infection.

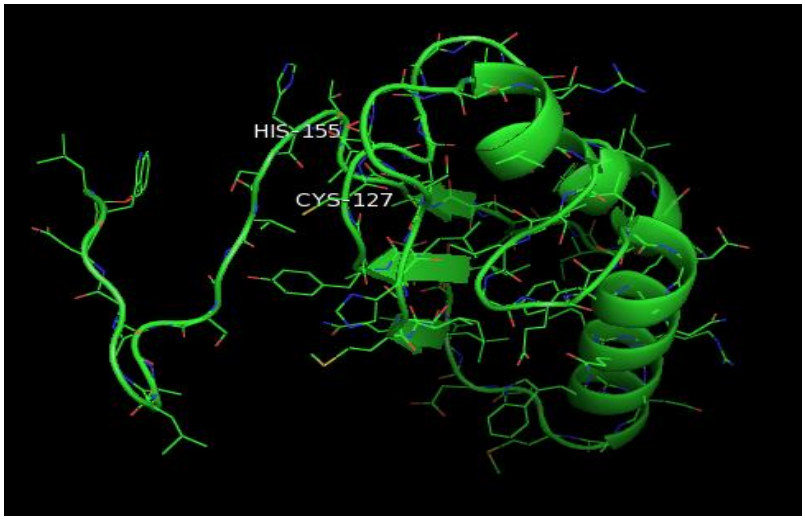

Figure 12. The 181 amino acids modeled from the domain of unknown function 4347 (pfam14252) in BAV1945 using Phyre[2]. 87 residues (48%) were modeled with 91% confidence using the highest scoring template, a cysteine protease domain in *C. difficile* (c3pa8A). Conserved histidine and cysteine residues predicted to reside in catalytic site were highlighted.

RTX toxins have been found to perform a range of functions including pore formation in host cell membranes, bacterial growth inhibition, and contribution to surface defense mechanisms (Linhartova, 2010). $MARTX_{VC}$ and TcdA/B have glycosyltransferase domains that modify and inactivate host Rho-GTPases (Sheahan, 2007 and reviewed by Schirmer, 2004). $MARTX_{VC}$ can also directly cross-link monomeric actin, eliminating the host's ability in forming functional actin filaments (Cordero, 2006). Both of these activities disrupt the cytoskeletal arrangement of the host cell leading to cell rounding (Fullner, 2001). An N-terminal adenylate cyclase (AC) domain in ACT catalyzes the conversion of ATP to cAMP (Rogel, 1991) upon binding of host cytosolic calmodulin (Shen, 2002). The AC domain is responsible for deactivation of the RhoA-GTPase in macrophages, resulting in dysfunctional actin assembly and overall inhibition of immunogenic activity (reviewed by Carbonetti, 2010). No host effector

domains have been identified in either BAV1944 or BAV1945. As BAV1945 fits the model of a multifunctional RTX toxin better than BAV1944, we predict that there is a novel effector domain within this protein. We are currently investigating the effects of *B. avium* lysate on the actin assembly of cultured turkey fibroblasts.

The *B. avium* and *Achromobacter* RTX-like proteins may represent a novel group of large RTX toxins. This possibility would explain why the Δ*bav1944-5* mutant was not deficient in traditional phenotypes associated with *B. avium* virulence. BAV1944 and BAV1945 share common features to RTX-toxins such as a TISS, GD-rich nonapeptide repeats, and a cysteine protease domain. Further work needs to be done to identify any potential host effects of BAV1944 and BAV1945. Recombinant BAV1944 and/or BAV1945 carrying antigenic sequences from other virulence factors could be used as vaccine subunits to induce a more controlled and site-directed immune response. From these insights we have generated a model BAV1944/BAV1945 translocation and activity (Fig. 13). This model may inform future studies in the lab, based on the findings in this thesis.

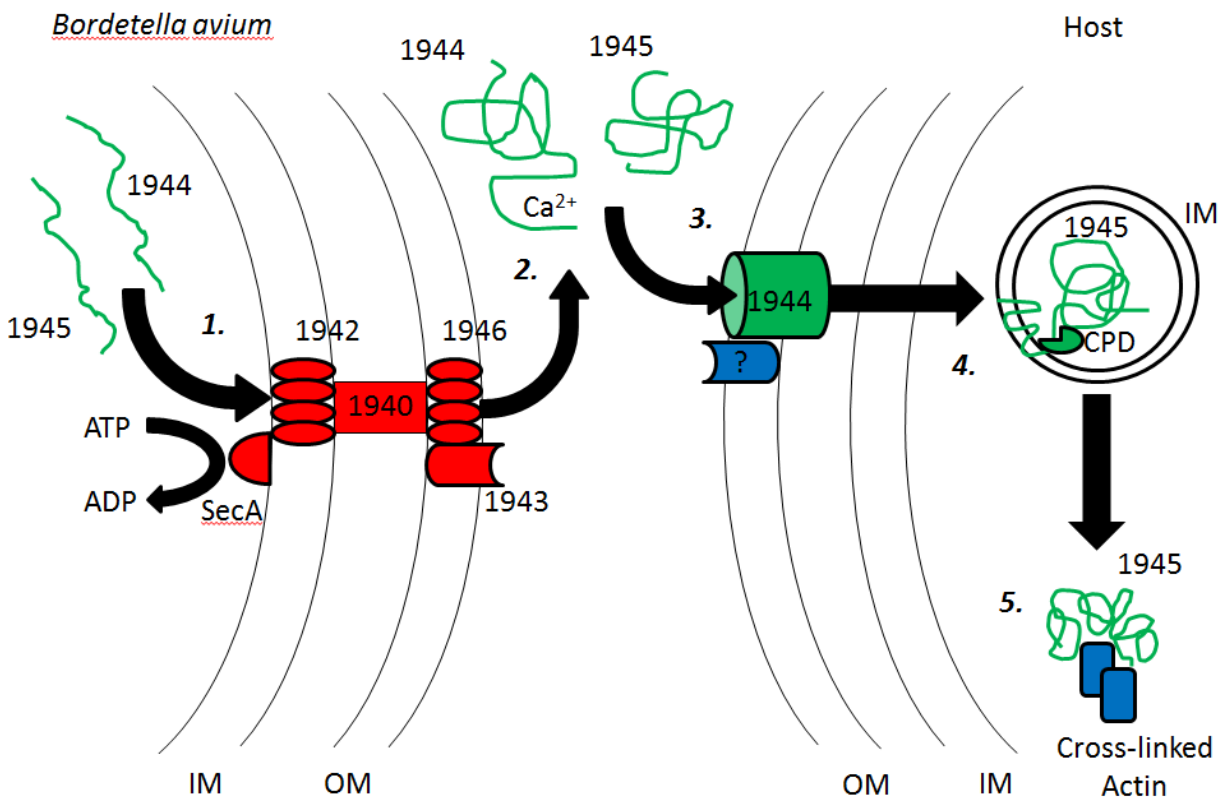

Figure 13. A potential model for BAV1944 and BAV1945 secretion, translocation, and activity. *Putative RTX toxins (green)* – 1945: multifunctional autocatalytic RTX toxin; 1944: pore forming RTX toxin; Ca^{2+}: 1944 calcium binding domain; CPD: 1945 cysteine protease domain. *Putative TISS (red)* – SecA: ATB-binding motor protein; 1942: inner membrane protein used for secretion signal recognition; 1940: HlyD-like transmembrane protein; 1946: TolC-like outer membrane protein; 1943: signal transduction protein. *Other* – IM: inner membrane; OM: outer membrane; "?": unknown host receptor (blue); cross-linked actin (blue). *Steps* (italics) – 1. Secretion of BAV1944 and BAV1945; 2. Calcium induced folding of BAV1944; 3. Membrane embedding of BAV1944 and endocytosis of BAV1945. 4. BAV1945 release through CPD processing; 5. BAV1945 actin cross-linking.

Supplemental Tables and Figures

Table 1. Bacterial strains and plasmids.

Strain or plasmid	Description	Source or reference
***B. avium* strains**		
197N	Parental strain; Dnt+ Hag+ Mot+ Nal^R	(Temple, 1998)
197N-2	Parental except for Str^R	(Temple, 2010)
***E. coli* strains**		
DH5α	Cloning strain	Invitrogen
Top10	Cloning strain	NEB
MC4100λPir	Host for pKAS46	(Skorupski, 1996)
MM294	Host for pRK2013	(Figurski, 1979)
T7 Express *lysY*	T7 expression strain	NEB
Plasmids		
pCR2.1	Cloning plasmid Amp^R Kan^R	Invitrogen
pKAS46	Mobilizable cloning plasmid Kan^R Str^S	(Skorupski, 1996)
pRK2013	Mobilization plasmid Kan^R	(Figurski, 1979)
pUC57	Cloning plasmid Amp^R	GenScript
pGS-21a	Expression plasmid Amp^R	GenScript

Table 2. Primer sequences for Δ*1944-5* knock-out mutagenesis and RT-PCR of *bav1945* and *bav1940* (TISS). Underlined sequences represent *Asc*I site.

Primer set	Left sequence (5'->3')	Right sequence (5'->3')
Knock-out mutant		
bav1944-45 upstream	CAAAGCCGCCTGTTGCTC	TTCTCGGCCATCAAGGGCGGCG CGCCCGGCCGTATCCAGTCTTTCTC
bav1944-45 downstream	AAAGACTGGATACGGCCGGGCG CGCCGCCCTTGATGGCCGAGAAATC	AAGAAACTGGCACGCAAACT
Internal Δ*1944-45*	ATCGTCTGGGTGATGAGGTC	TTCGCTTTCGCTAGGTTCTG
RT-PCR		
bav1940 cDNA	CTGTTGGAGGCGCTGGTAGAG	TCGGCGTTGTCGTCATCCAC
bav1945 cDNA	GCCATGACGGTAATCCAGCAG	ACACTTGGCGAGTCGATGTCC

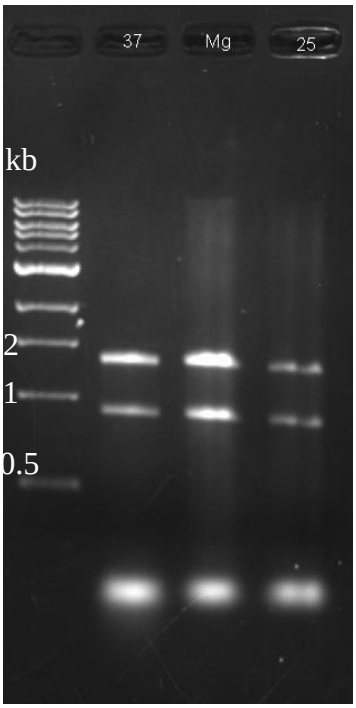

Figure S1. RNA extracted from *B. avium* grown at 37°C with or without 20mM $MgSO_4$ (lanes 2 and 3) or at 25°C (lane 4). The bands at approximately 1 and 2 kb represent the 18S and 28S ribosomal RNA fragments respectively. A molecular weight standard was run in lane 1 with labelled bands at 0.5, 1, and 2 kb.

Note RNA was also extracted from cultures grown with $MgSO_4$ or at 25°C for comparison of *bav1945* and *bav1940* expression. These conditions have been associated with downregulation of virulence factors in *B. avium*. However, products of approximately 0.6 kb and 0.8 kb were amplified in these samples using primers for *bav1945* and *bav1940* respectively (Fig. S2). The presence of positive PCR products in the extracted RNA from $MgSO_4$ and 25°C indicated genomic DNA contamination, which could not be eliminated through DNase treatment.

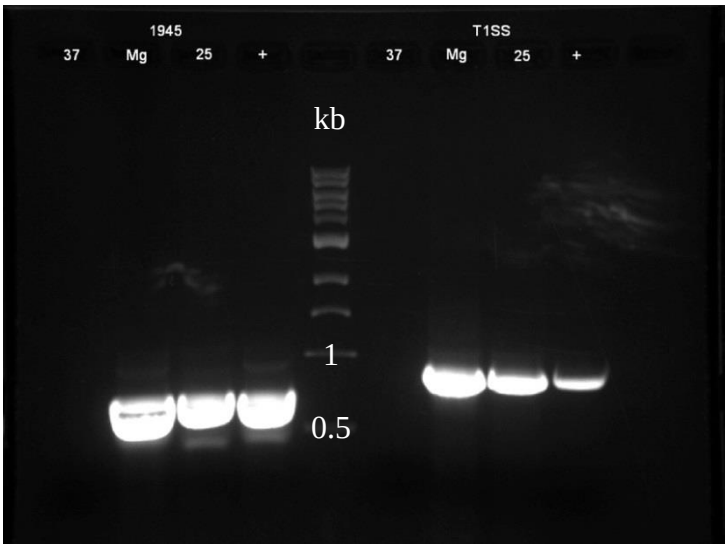

Figure S2. PCR check of processed RNA for genomic DNA contamination. Lanes 1-3 represent RNA samples tested with primers for *bav1945*, while lanes 6-9 represent RNA samples tested with primers for *bav1940* (TISS). RNA was extracted from cultures grown at 37°C with or without 20mM $MgSO_4$ or at 25°C. The positive control lanes (+) contain genomic DNA amplified with the *bav1945* or *bav1940* primer sets. A molecular weight standard was run in lane 5 with labelled bands at 0.5 and 1 kb.

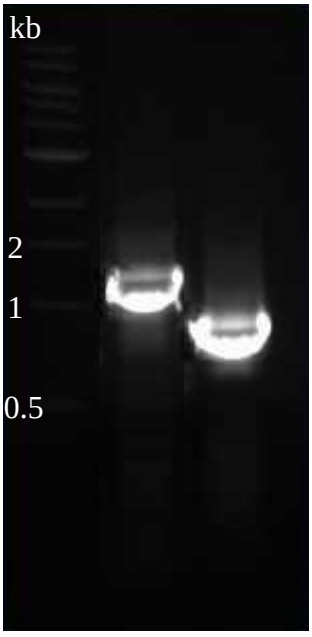

Figure S3. Primary PCR of upstream (lane 2) and downstream (lane 3) coding elements of the *bav1944-5* locus. A molecular weight standard was run in lane 1 with labelled bands at 0.5, 1, and 2 kb.

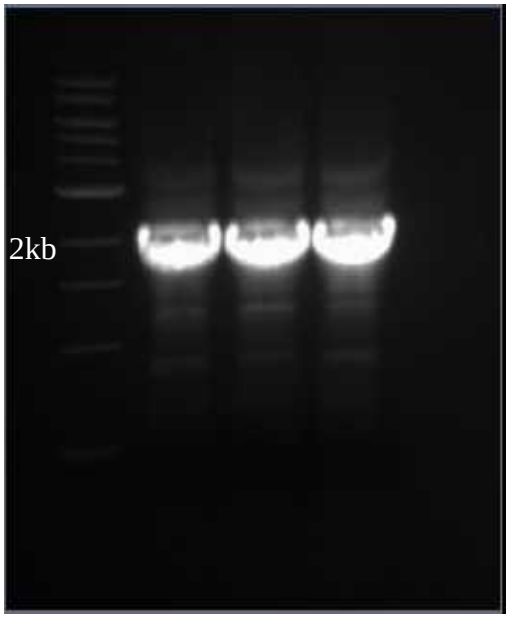

Figure S4. Secondary splice-by-overlap extension PCR of the upstream and downstream *bav1944-5* coding elements (lanes 2-4). A molecular weight standard was run in lane 1 with the band at 2 kb labelled.

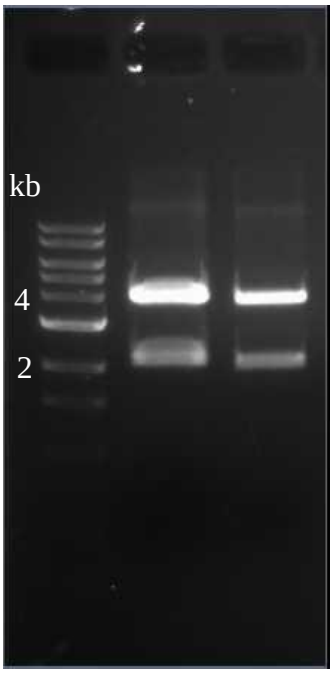

Figure S5. Restriction digest of pTOPO (Δ*bav1944-5*) with *Eco*RI (lanes 2 and 3). The bands at approximately 2 and 4 kb represent the digested insert and vector respectively. A molecular weight standard was run in lane 1 with labelled bands at 2 and 4 kb.

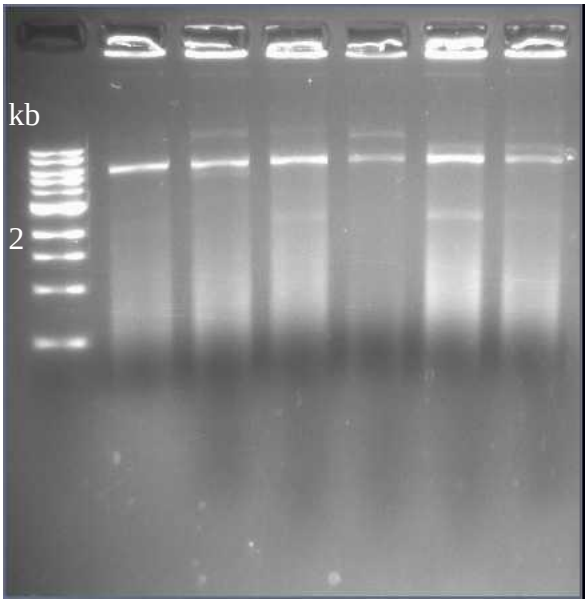

Figure S6. Restriction digest of pKAS46 (Δ*bav1944-5*) extracted from various colonies with *Eco*RI (lanes 2-7). The bands at approximately 2 and 6 kb represent the digested insert and vector respectively. Lanes 4 and 6 contain samples with released insert. A molecular weight standard was run in lane 1 with the band at 2 kb labelled.

REFERENCES

1. **Adem, A., S. Stockwell, K. Cresawn, and L. Temple.** 2011. Functional characterization of novel surface proteins in *Bordetella avium*. Senior Honors Thesis. James Madison University.
2. **Arp, L. H., and N. F. Cheville.** 1984. Tracheal lesions in young turkeys infected with *Bordetella avium*. *Am. J. Vet. Res*. **45**: 2196–2201.
3. **Baumann, U., S. Wu, K. M. Flaherty, and D. B. McKay**. 1993. Three dimensional structure of the alkaline protease of *Pseudomonas aeruginosa*: a two-domain protein with a calcium binding parallel beta roll motif. *EMBO J*. **12**:3357–3364.
4. **Boardman, B. K., and K. J. Satchell.** 2004. *Vibrio cholera* strains with mutations in an atypical type I secretion system accumulate RTX toxin intracellularly. *J. Bacteriol*. **186**: 8137–8143.
5. **Carbonetti, N. H.** 2010. Pertussis toxin and adenylate cyclase toxin: key virulence factors of Bordetella pertussis and cell biology tools. *Fut. Mic*. **5**: 455-469.
6. **Cordero, C.L., D.S. Kudryashov, E. Relsler, and K.J. Fullner.** 2006. The actin cross-linking domain of the *Vibrio cholerae* RTX toxin directly catalyzes the covalent cross-linking of actin. *J. Biol. Chem.* **281**: 32366-32374.
7. **DeLey, J., P. Seger, K. Kersters, W. Mannheim, and A. Lievens.** 1986. Intra and intergeneric similarities of the *Bordetella* ribosomal ribonucleic acid cistrons: proposal for a new family, *Alcaligenaceae*. *Int. J. Syst. Bacteriol*. **36:** 405–414.
8. **Figurski, D.H. and D.R. Helinski.** 1979. Replication of an origin-containing derivative of plasmid RK2 dependent on a plasmid function provided in *trans*. *Proc. Natl. Acad. Sci*. **76:** 1648-1652.
9. **Fullner, K.J. and J.J. Mekalanos.** 2000. *In vivo* covalent cross-linking of cellular actin by the *Vibrio cholera* RTX toxin. *EMBO J*. **20:** 5315-5323.
10. **Fullner, K.J. W.I. Lencer, and J.J. Mekalanos.** 2001. *Vibrio cholerae*-induced cellular responses of polarized T84 intestinal epithelial cells are dependent on production of cholera toxin and the RTX toxin. *Infect. Immun*. **69:** 6310-6317.
11. **Gentry-Weeks, C. R., et al.** 1988. Dermonecrotic toxin and tracheal cytotoxin, putative virulence factors of *Bordetella avium*. *Infect. Immun*. **56:** 1698–1707.
12. **Gentschev I., J. Hess, and W. Goebel.** 1990. Change in the cellular localization of alkaline phosphatase by alteration of its carboxy-terminal sequence. *Mol Gen Genet* **222**: 211–216.
13. **Gray, M. C., W. Ross, K. Kim, E. J. Hewlett**. 1999. Characterization of binding of adenylate cyclase toxin to target cells by flow cytometry. *Infect. Immun.* **67**: 4393-4399.
14. **Holland, I. B., M. A. Blight, B. Kenny.** 1990. The mechanism of secretion of hemolysin and other polypeptides from gram-negative bacteria. *J. Bioenerg. Biomem*. **22**: 473-491.
15. **Holm, H.A.** 2000. Rapid automatic detection and alignment of repeats in protein sequences. *Proteins*. **41**: 224-237.
16. **Jackwood, M. W., S. McCarter, and T. Brown.** 1995. *Bordetella avium*: an opportunistic pathogen in Leghorn chickens. *Avian Dis*. **39**: 360-367.
17. **Jackwood, M. W., and Y. M. Saif.** 2003. Bordetellosis, p. 705–718. *In* Y. M. Saif, H. J. Barnes, J. R. Glisson, A. M. Fadly, L. R. McDougal, and D. E. Swayne (ed.), Diseases of poultry, 11th ed. Iowa State University Press, Ames, IA.

18. **Kamanova, J., O. Kofronova, J. Masin, H. Genth, J. Vojtova, I. Linhartova, O. Benada, I. Just, and P. Sebo.** 2008. Adenylate cyclase toxin subverts phagocyte function by RhoA inhibition and unproductive ruffling. *J. Immunol*. **181**: 5587-5597.
19. **Kelley L.A. and M.J. Sternberg.** 2009. Protein structure prediction on the web: a case study using the Phyre server. *Nat. Prot*. **4**: 363-371.
20. **Kuehne, S.A., S.T. Cartman, J.T. Heap, M.L. Kelley, A. Cockayne, and N.P. Minton.** 2010. The role of toxin A and toxin B in *Clostridium difficile* infection. *Nat*. **467**: 711-714.
21. **Ladant, D., and A. Ullmann**. 1999. Bordetella pertussis adenylate cyclase: a toxin with multiple talents. *Trends Microbiol*. **7**:172–176.
22. **Linhartova, I., et al.** 2010. RTX proteins: a highly diverse family secreted by a common mechanism. *FEMS Microbiol*. *Rev.* 34:1076-1112.
23. **Lupardus, P. J., et al.** 2008. Small molecule induced allosteric activation of the *Vibrio cholerae* RTX cysteine protease domain. *Sci*. **322**: 265-268.
24. **Miyamoto, D. H., et al.** 2011. *Bordetella avium* causes induction of apoptosis and nitric oxide synthase in turkey tracheal explant cultures. *Mic. Infect*. **13**: 871–879.
25. **Morova J, R. Osicka, J. Masin, and P. Sebo**. 2008. RTX cytotoxins recognize beta2 integrin receptors through N-linked oligosaccharides. *P. Natl. Acad. Sci.* **105**: 5355–5360.
26. **Naylor, C. E., et al.** 1999. Characterization of calcium-binding C-terminal domain oc *Clostridium perfringens* alpha-toxin. *J. Mol. Biol*. **294**: 757-770.
27. **Pimenta, A.L., K. Racher, I.B. Holland, et. al.**. 2005. Mutations in HlyD, part of the type 1 translocator for hemolysin secretion, affect the folding of the secreted toxin. *J. Bacteriol*. **187**: 7471-7481.
28. **Pitman, M.** 1974. Genus *Bordetella*, p. 282–283. *In* R. E. Buchanan, and N. E. Gibbons (ed.), Bergey's manual of determinative bacteriology, 8th ed. The Williams and Wilkins Co., Baltimore, Md.
29. **Prochazkova K. and K.J. Satchell.** 2008. Structure-function analysis of inositol hexakisphosphate-induced autoprocessing of the *Vibrio cholerae* multifunctional autoprocessing RTX toxin. *J. Biol. Chem*. **283**: 23656-23664.
30. **Reineke, J., et al**. 2007. Autocatalytic cleavage of *Clostridium difficile* toxin B. *Nat*. **446**: 415-419.
31. **Rhea, L. J.** 1915. The comparative pathology of the tracheal and bronchial lesions produced in man by *B. pertussis* (whooping cough) and those produce in dogs by *B. bronchiseptica* (canine distemper). *J. Med. Res*. **32**: 471–474.
32. **Rogel, A., R. Meller, E. Hanski.** 1991. Adenylate cyclase toxin from *Bordetella pertussis*. *J. Biol. Chem*. **266**: 3154-3161.
33. **Rose T, Sebo P, Bellalou J, Ladant D.** 1995. Interaction of calcium with *Bordetella pertussis* adenylate cyclase toxin. Characterization of multiple calcium-binding sites and calcium-induced conformational changes. *J. Biol. Chem*. **270**: 26370 –26376.
34. **Rupnik, M., S. Pabst, M. Rupnik, C. Eichel-Streiber, H. Urlaub, and H. Soling.** 2005. Characterization of the cleavage site and function of resulting cleavage fragments after limited proteolysis of *Clostridium difficile* toxin B (TcdB) by host cells. *Microbiol*. **151**: 199-208.
35. **Satchell, K.J.** 2007. MARTX, multifunctional autoprocessing repeats-in-toxin toxins. *Infect. Immun*. **75**: 5079–5084.

36. **Schirmer, J. and K. Aktories**. 2004. Large clostridial cytotoxins: cellular biology of rho/ras-glucosylating toxins. *Biochim. Biophys. Acta*. **1673**: 66-74.
37. **Sebaihia, M., et al.** 2006. Comparison of the genome sequence of the poultry pathogen *Bordetella avium* with those of *B. bronchiseptica*, *B. pertussis*, and *B. parapertussis* reveals extensive diversity in surface structures associated with host interaction. *J. Bacteriol*. **188**: 6002–6015.
38. **Sheahan, K., C.L. Cordero, and K.J. Satchell**. 2007. Autoprocessing of the *Vibrio cholerae* RTX toxin by the cysteine protease domain. *EMBO. J*. **26**: 2552-2561.
39. **Sheahan, K. and K.J. Satchell**. 2007. Inactivation of small Rho GTPases by the multifunction RTX toxin from *Vibrio cholerae*. *Cell. Micro*. **9**: 1324-1335.
40. **Shen, Y., et. al.** 2002. Physiological calcium concentrations regulate calmodulin binding and catalysis of adenylyl cyclase exotoxins. *EMBO*. **21**: 6721-6732.
41. **Shen, Y., P.J. Lupardus, V.E. Albrow, A. Guzzetta, J.C. Powers, C. Garcia, and M. Bogyo.** 2009. Mechanistic and structural insights into the proteolytic activation of Vibrio cholera MARTX toxin. *Nat. Chem. Biol*. **5**: 469-478.
42. **Skeeles, J. K., and L. H. Arp.** 1997. Bordetellosis (turkey coryza), p. 275–288. In B. W. Calnek, H. J. Barnes, C. W. Beard, L. R. McDougal, and Y. M. Saif (ed.), Diseases of poultry. Iowa State University Press, Ames.
43. **Skorupski K. and R.K. Taylor.** 1996. Positive selection vectors for allelic exchange. *Gene*. **169**: 47-52.
44. **Song, L., M.R. Hobaugh, C. Shustak, S. Cheley, H. Bayley, and J.E. Gouaux.** 1996. Structure of staphylococcal alpha-hemolysin, a heptameric transmembrane pore. *Sci*. **274**: 1859-1866.
45. **Temple, L.M., et al.** 2010. Identification and characterization of two *Bordetella avium* gene products required for hemagglutination. *Infect. Immun*. **78**: 2370-2376.
46. **Tseng, T., B.M. Tyler, and J.C. Setubal**. 2009. Protein secretion systems in bacterial-host associations, and their description in the gene ontology. *BMC Microbiol*. **9**: 1-9.
47. **Weiss, J.B., P.H. Ray, and P.J. Bassford Jr**. 1988. Purified SecB protein of *Escherichia coli* retards folding and promotes translocation of the maltose-binding protein *in vitro*. *Proc. Natl. Acad. Sci*. **85**: 8978-8982.
48. **Zhang, Y.** 2008. I-TASSER server for protein 3D structure prediction. *BMC Bioinfor*. **9**: 40.